*Nanotechnology Perceptions*
*ISSN 1660-6795*
*www.nano-ntp.com*

# Synthesis and Characterisation of Palladium Doped Ga2O3 Nanoparticles as a Potent Microbiome Growth Inhibitor of Healthcare Waste

**Kiran Kore[1], Dr. Suman Dabbu[1], Dr. Someshwar Pola[2*], Dr. Vasundhara Mutta[3], Akbar Pasha[4]**

*[1]Department of Biomedical Engineering, University College of Engineering, Osmania University, Hyderabad - 500007, Telangana, India.*
*[2]Department of Chemistry, University College of Science, Osmania University, Hyderabad - 500007, Telangana, India.*
*[3]Polymers and Functional Materials Department, CSIR-Indian Institute of Chemical Technology, Hyderabad-500007, Telangana, India.*
*[4]Department of Genetics, Osmania University, Hyderabad - 500007, Telangana, India*
*Email: somesh.pola@gmail.com*

Biomedical waste (BMW) presents a significant global challenge due to its potential adverse effects on human health and the environment and there are inadequate resources to address it. In this study, we synthesized Pd-doped $Ga_2O_3$ nanoParticles (NPs) using a sol-gel method and investigated their influence on BMW management; this is the first of its type. In addition, the synthesized NPs were characterized using Fourier transform infrared (FTIR) spectra, an X-ray diffractometer (XRD), a scanning electron microscope (SEM), and UV-visible spectroscopy. The X-ray diffraction (XRD) analysis reveals that the Pd-$Ga_2O_3$ nanoparticles crystallize in a single-phase monoclinic structure, with an average crystallite size determined to be 15.11 nm.FTIR spectra reveal the molecules and bonding associated with the developed NPs and confirms Pd capping on the surface of $Ga_2O_3$ NPs. The SEM results revealed the formation of angular-shaped NPs with a minimum size of 10 nm. The UV-visible absorption spectra shows that the produced Pd-doped $Ga_2O_3$ composite has a band gap of 4.178 eV, which is less extensive than that of the earlier reported values. The importance and relevance of this work is on the photocatalytic activity of the developed Pd-$Ga_2O_3$ NPs which shows substantial antibacterial activity against hospital waste and considerably suppressed microbial growth. Overall, Pd-$Ga_2O_3$ NPs developed in this work can be utilized to control biomedical waste and there by decrease environmental pollution.

**Keywords:** Biomedical waste, Pd-doped $Ga_2O_3$, characterisation, photocatalytic activity, anti-bacterial activity.

## 1. Introduction

Healthcare waste generation is a significant global concern due to its potential influence on the environment and human health. The increasing global population results in a large increase in biomedical waste (BMW) production, and there are insufficient resources to cope with it (1). Hospitals are an important reservoir of microcontaminants owing to diagnostic, laboratory, and research operations, as well as patient excretion of medications. Pharmaceuticals and metabolites, chemicals, heavy metals, disinfecting agents, endoscope and instrument detergents, radioactive tags, and iodinated contrast media are examples of active components of BMW (2). Globally, developed countries generate up to 0.5 kg of hazardous medical waste per hospital bed each day, while low-income nations produce around 0.2 kg per hospital bed per day (3). According to data released by the Central Pollution Control Board (CPCB) in 2022, India generates a total of 507 tonnes of biomedical waste (BMW) per day. The country is home to 393,939 healthcare facilities (HCFs), including 129,259 bedded facilities and 267,155 non-bedded facilities, all contributing to BMW production. To manage this waste, there are 218 operational common biomedical waste treatment facilities (CBWTFs) across the country, with an additional 34 facilities currently under development (4). A possible cause of infection is BMW that is not appropriately managed or treated. The disposal and subsequent treatment of waste produced within the healthcare system can introduce pathogens and hazardous substances into the ecosystem, thereby posing potential health risks (1). According to published research, over 40 different types of harmful microorganisms have the potential to spread and infect individuals. In addition to reducing the risk of hospital-acquired infections, careful treatment and management of BMW can reduce the transmission of diseases (5). Standard management techniques include reducing waste storage and transportation, recycling, reusing, and processing through a variety of treatment technologies such as thermal, chemical, as well as irradiation methods, biological processes, disinfection, and sterilization (6). The risks associated with BMW underscore the critical need for effective waste management systems and sustained initiatives to mitigate their negative impacts on both environmental and human health. Effective disposal and treatment of BMW is vital to minimizing these risks and conserving the environment and public health.

Nanotechnology has recently become a prominent advancement in the environmental protection sector, especially in the field of waste management. This technology employs nanoparticles (NPs) (materials with at least one dimension smaller than 100 nanometres), which have excellent adsorption, oxidation/reduction, and catalytic activity for a variety of pollutants, including heavy metals, organics, and inorganic contaminants (7). Nanoparticles (NPs) are synthesized from a diverse range of materials, which can be categorized into three distinct types: organic, carbon-based, and inorganic. Organic NPs are lipid NPs (micells and liposomes), as well as polymeric NPs (dendrimers, ferritin, and hydrogel), these nanoparticles are biocompatible and are predominantly utilized in the biomedical field for targeted drug delivery applications (8). Carbon-based NPs, including carbon nanotubes and quantum dots, are employed in sensor technology and bioimaging. In contrast, metal-based nanoparticles, synthesized from metal precursors and classified as monometallic, bimetallic, or polymetallic, are utilized across a wide range of applications, including tissue repair, immunoassays, antimicrobial materials, diagnostics, as well as health and environmental applications (9,10).

In recent years, metal NPs have garnered significant interest due to their exceptional

antimicrobial activity against a broad range of bacteria and fungi. Among these, metal nanoparticles such as silver (Ag), gold (Au), copper (Cu), palladium (Pd), platinum (Pt), and titanium (Ti), as well as metal oxide NPs including $Fe_3O_4$, $TiO_2$, CuO, and ZnO, are the focus of extensive research (11–14). These NPs hold considerable promise as antibacterial agents across various sectors, including textiles, skincare, biomedicine, and food additives. Their potential is attributed to their cost-effectiveness, size-dependent antimicrobial efficacy against a wide range of microorganisms, and relatively low cytotoxicity to human cells (15).

The development of nanostructured oxides made up of two or more metallic components is one of the most recent advances in the nanotechnology of metal oxides. Due to their unique electrical, optical, magnetic, and other physicochemical features, they offer a vast range of potential applications. Multi-metal oxide NPs, such as ZnxMg1−xO, Ta-doped ZnO, and Ag/$Fe_3O_4$, Zn-CuO, $ZnTiO_3$, ZnO-$TiO_2$, etc. nanocomposites, are being extensively studied as possible antibacterial agents due to their positive synergistic effects (16). Of these, gallium oxide ($Ga_2O_3$) NPs are unique in optics, photoelectric conversion, and electrical sectors. $Ga_2O_3$ materials can be synthesized using a variety of methods including hydrothermal, sol-gel, and chemical bath etc. It has been shown to possess several polymorphs (α, β, γ, δ and ε-$Ga_2O_3$) and has good physical and chemical properties (17,18). These materials are widely used in a variety of fields, including gas sensors, UV detection, flat panel displays, photocatalysis, UV filters, and optoelectronic devices (19–21). Reddy et al., reported that, β-$Ga_2O_3$ exhibited higher photoactivity than α and γ crystalline states (22). The wide band gap semiconductor β-$Ga_2O_3$ (Eg=4.9eV) is UV responsive and a potential material for photocatalysis, including the degradation of organic substances (23), for the degradation of dyes (24), and water splitting etc, (25). Doping β-$Ga_2O_3$ with specific metal ions may significantly change its physical and electrical properties, allowing for customised device applications. Doping β-$Ga_2O_3$ with Sn, Cr, Ti, Mn, and Mo etc. results in variations in optical absorption and band gap (26–29). Recent studies have shown that doping specific metal ions, such as Ni, Zn, and Pb, improves the photocatalytic activity of $Ga_2O_3$ (30–32). However, the photocatalytic properties of these materials have not been the primary focus of several studies.

In this study, we examined the enhancement of photocatalytic performance in $Ga_2O_3$ through the incorporation of metal ions, specifically palladium (Pd). We present findings on how the addition of these metal ions influences the photocatalytic activity of $Ga_2O_3$, particularly concerning the overall degradation of biomedical waste generated by microbiomes. To characterize the structural properties and functional groups of the synthesized Pd-$Ga_2O_3$, we employed X-ray diffraction (XRD), Fourier transform infrared spectroscopy (FT-IR), and scanning electron microscopy (SEM). Additionally, the photocatalytic performance of the Pd-$Ga_2O_3$ nanorods was assessed through UV-visible absorption spectroscopy.

## 2. Materials and Methods

### 2.1 Synthesis of Pd-doped $Ga_2O_3$ NPs

New Pd-doped $Ga_2O_3$ Nps were synthesized using the sol-gel method. 0.5 g of $PdCl_2$ was dissolved in a 1:10 mixture of ethanol and water, and 4.8 g of $Ga_2O_3$ solid was suspended. The solvent (50%) was then evaporated on the hot plate by continuous stirring with a magnetic

stirrer, followed by the addition of 25 mL of ethylene glycol and continued burning to produce the black xerogel. The resultant xerogel was calcined at 750°C for approximately 4 hours, yielding a light brown dry powder. The resultant powder was absolutely crushed and analysed using spectroscopic analysis.

2.2 Characterisation of Pd doped $Ga_2O_3$ NPs

The crystalline structure of synthesized Pd-$Ga_2O_3$ NPs were studied using a Shimadzu XRD-7000 diffractometer with a voltage of 40kV, current of 30mA, and a 2θ (Bragg angle) ranging from 5°-80°. For FTIR (Fourier transform infrared Spectrophotometer) measurement, the pellet was formed through the mixture of Pd-doped $Ga_2O_3$ NPs and FTIR graded potassium bromide in a 1:100 ratio. The sample pellets were placed in the sample holder, and the FTIR spectrum was recorded using a Nexus 670 ThermoNicolet FTIR with a resolution of 4 $cm^{-1}$ within the 400 to 4000 $cm^{-1}$ range. Scanning electron microscopy (Carl Zeiss-6027) was used for assessing size and surface morphology. To eliminate impurities, the material was filtered using Millipore 0.2 µm filters. Subsequently, the sample was mounted onto a stub and coated with Pt for scanning electron microscopy (SEM) analysis. The optical properties were evaluated using spectrophotometry (Rayleigh UV-2100) measurement in the wavelength range of 200–800 nm.

2.3 Anti-bacterial activity of Pd-$Ga_2O_3$

The antibacterial activity of Pd-$Ga_2O_3$ NPs was examined using agar spread plate method. In order to perform the investigation, biomedical waste—such as solid and/or liquid waste and any intermediate product—that is produced during the diagnosis, treatment, or immunization of individuals was carefully collected from Srikara hospital. A 5 mL aliquot of the sample was mixed with 100 mL of distilled water prior to processing. From this homogeneous solution, 1 mL was taken and treated with 1 mL of synthesized Pd-doped $Ga_2O_3$ NPs (5 mg/mL). The mixture was then serially diluted using sterile distilled water up to a dilution factor of $10^4$. Additionally, a 1 mL aliquot of the homogenous solution was withdrawn and serially diluted up to a $10^4$ dilution factor using sterile distilled water. This served as the untreated control, corresponding to the serially diluted treated samples described above. A 100 µL aliquot from each dilution, both treated and untreated, was inoculated onto Mueller-Hinton agar using sterile cotton swabs and spread plate technique to obtain pure cultures. After 24 h of incubation at 37°C the colonies were observed and counted using ImageJ software (NIH, Version 1.50i, USA).

2.4 Statistical analysis

For assessing statistical differences, ANOVA was employed. Statistical analyses were performed using GraphPad Prism 8.4.2, with a significance level of $P < 0.05$.

## 3. Results and Discussion

3.1 XRD-analysis of Pd-$Ga_2O_3$

The synthesized Pd-$Ga_2O_3$ NPs were subjected to X-ray diffraction to assess crystallinity and average particle size. The X-ray diffraction patterns of the synthesized Pd-$Ga_2O_3$ NPs are illustrated in Fig. 1. The diffraction peaks observed in the Pd-doped $Ga_2O_3$ sample were in

accordance with the crystalline monoclinic crystal structures of PdO (Palladium oxide) (JCPDS 96-200-2238) and $Ga_2O_3$ (JCPDS 96-200-4988) (33), with well-defined, sharp peaks found at 2θ = 30.02°, 31.62°, 33.6°, 35.16°, 38.42°, 45.78°, 60.98°, and 64.66°, which corresponded to the crystal planes (400), (-202), (-111), (111), (-311), (-312), (020) and (040), respectively. Earlier studies have demonstrated that calcining at a high temperature produced β-$Ga_2O_3$ nanorods with a high crystalline quality, as evidenced by the distinctly increased XRD patterns with sharp peaks. The prominent and distinct peaks were detected at 2θ=30.4, 31.8, 35.3, and 64.71° (22). The acquired data was supplemented with regular standard Miller indices, indicating that the result is of Pd-$Ga_2O_3$ NPs with a monoclinic crystalline structure, which coincides with earlier reported data and also fits the literature values well (34,35).

The Scherrer equation was utilized to calculate the average crystallite size of Pd-$Ga_2O_3$ NPs (NPs):

$$D = \frac{k\lambda}{\beta \cos \theta}$$

Where D is the average particle size, k is the Scherrer constant, which is usually 0.9, λ is the wavelength of X-rays, β is the full width at half maximum (FWHM) of an observed peak, and θ is the Bragg diffraction angle. El-Fatah et al. reported that the average size of $Ga_2O_3$ NPs was 30.2 nm, and the XRD pattern revealed that gallium-oxide NPs formed in a single-phase structure (36). Doping of NPS with other elements can increase the optical characteristics of materials used in optoelectronics and photocatalytic applications. For pure β-$Ga_2O_3$ and 3at% β-$Ga_2O_3$ particles, the average crystallite size is estimated to be around 76 nm and 51 nm, respectively (35). Doping with Pd reduced the crystallite size of produced Mn3O4. The estimated grain size values for pure and pd-doped Mn3O4 were around 32 and 28 nm, respectively (37). In the present study we synthesised pd-doped $Ga_2O_3$ NPs and the average crystallite size (D) of Pd-$Ga_2O_3$ particles is calculated to be 15.11 nm. The catalytic activity of NPs has been found to increase as the NP size is decreased and the findings suggest that the smaller particle size formed due to the ionic radii of the Pd (0.137 nm) is greater than that of Ga (0.1218 nm) (38).

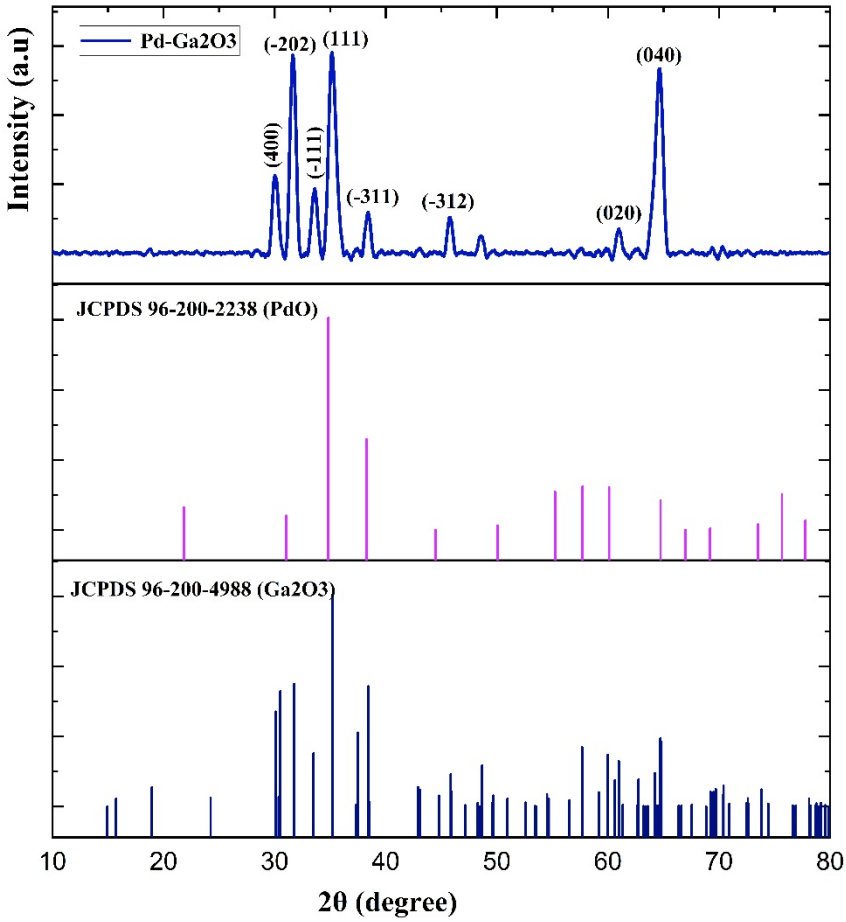


Figure 1: X-ray diffraction (XRD) pattern of Pd-$Ga_2O_3$, indexed with JCPDS 96-200-4988 ($Ga_2O_3$) and JCPDS 96-200-2238 (PdO).

3.2 FTIR spectrum of Pd-$Ga_2O_3$

The composition and quality, as well as the functional analysis of Pd-$Ga_2O_3$ NPs, were determined using an FTIR spectrum in the 400-4000 cm-1 region, as shown in Fig.2. The region of 3000–3700 cm-1 showed a wide absorption band, and the band at 3447 cm-1 corresponds to H–O–H stretching vibrations. A sharp peak observed at 1631 cm-1 is attributed to C=C stretching and bending vibrations of –OH groups and adsorbed water molecules. Strong peaks at 690 cm-1 and 474 cm-1 are associated with Ga–O bending vibrations. Thus, as determined by FTIR studies, Pd-$Ga_2O_3$ NPs are produced only in monoclinic structures. Similar findings have been reported for gallium oxide NPs used in the electrochemical detection of Pb2+, Cd2+, and Hg2+ ions in actual water, with FTIR absorption spectra of 3433, 1614, 688, and 459 cm−1 (36). The FTIR spectra of 3433 and 1614 cm−1 in the previously

mentioned findings displayed modest absorption peaks, whereas the results we obtained indicated strong and sharp peaks at 3447 and 1631cm-1, which correspond to the addition of palladium dopant (39). Reddy et al. reported that the weak stretching peaks of the Ga–O band were observed at 687, 577, and 468 cm-1 for α-$Ga_2O_3$ nanorods calcined at 500°C. On the other hand, the strong and narrow peaks at 659 and 441 cm−1 were clearly visible in the β-$Ga_2O_3$ nanorods that were calcined at high temperatures (1000 °C) (22). These FT-IR results closely matched the crystallinity trend for $Ga_2O_3$ nanorods with previously reported XRD data.

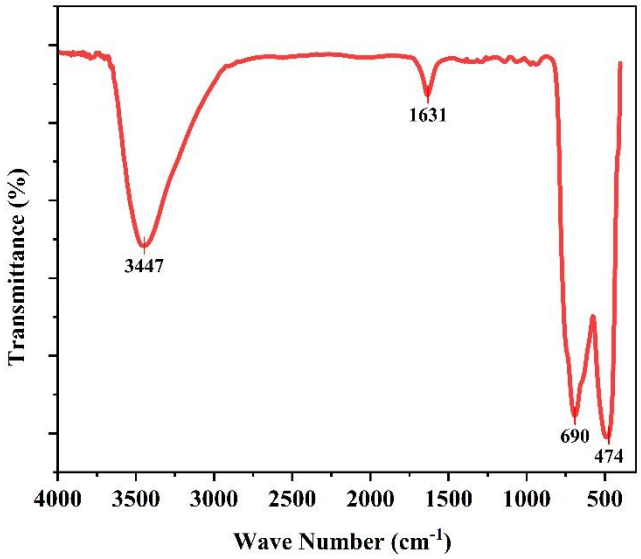


Figure 2: FTIR spectral analysis of Pd-$Ga_2O_3$ NPs

3.3 SEM analysis

The surface morphology of Pd-doped $Ga_2O_3$ NPs is illustrated in Fig 4. SEM analysis revealed that the morphological structure of the synthesized $Ga_2O_3$ nanostructure doped with Pd exhibits uneven surface topology (Fig. 3 A-C). The resulting particle size is less than 200 nm and clearly demonstrates a size range of 10-175 nm with an angular shape, indicating $Ga_2O_3$ NPs aggregation (Fig. 3A). The morphology of $Ga_2O_3$ NPs as detected by SEM analysis varies, with distinct morphologies reported on different substrates in the presence of silver, magnesium, indium, and other elements (35,40). Investigations using SEM analysis clearly indicate that pure β-$Ga_2O_3$ NPs with diameters of 20-270 nm and lengths reaching to many tens of micrometres (36,41,42). The size of NPs has specific characteristics that increase their photocatalytic activity, their compact size enhances their surface area, resulting in more efficient interaction with reacting substances and enhanced charge carrier motility (43). In this study, we obtained low-sized NPs (10 nm), which is an ideal catalytic characteristic of photocatalysts.

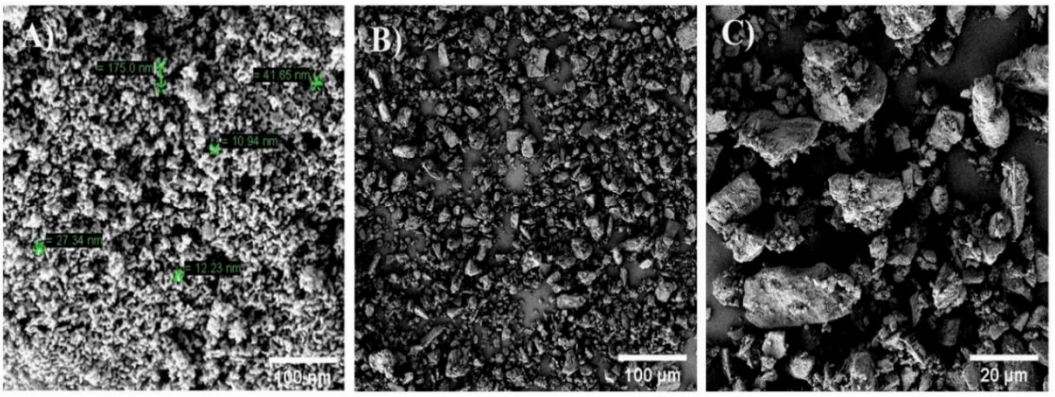


Figure 3: SEM images of synthesized $Ga_2O_3$ NPs doped with Palladium (Pd), A) 100 nm, B) 100 µm, C) 20 µm

3.4 UV-Visible absorption and band gap analysis

UV-Visible absorption spectroscopy is commonly used to analyse the optical characteristics of NPs based on their NP scale. A little variation in the size of NPs causes the surface plasmon resonance (SPR) or absorption band to shift. Figure 3A shows the absorption spectra of Pd-doped $Ga_2O_3$ composite. The findings of the UV-Vis spectroscopy showed that strong Pd-doped $Ga_2O_3$ absorption starts approximately 265 nm, which is the spectrum of UV-C radiation (Fig. 4A). Recent studies showed that the UV-vis absorbance spectra of pure β-$Ga_2O_3$ NPs demonstrate that the absorption onset of β-$Ga_2O_3$ is at around 270 nm (23,39). The prepared Pd-$Ga_2O_3$ displayed significant absorption in the UV spectral region below 400 nm, demonstrating the broad spectrum of the semiconductor material. This is due the surface plasmon resonance characteristic of Pd played a vital part in increasing light absorption (44).

The optical band-gap of Pd doped $Ga_2O_3$ composites determined using Tauc's model by using the Mott and Davis relation. The bandgap of these Pd-$Ga_2O_3$ was determined by plotting $(\alpha h\nu)^2$ vs photon energy. The bandgap (Eg) was determined by analyzing the transmittance curve and correlating it with the relevant equation (45,46).

$$(\alpha h\nu)^2 = B\,(h\nu - E_g)$$

Where α is the absorption coefficient, h is the Planck constant, ν is the photon frequency, Eg is the band gap energy, and B is a constant. A plot of $(\alpha h\nu)^2$ against photon energy is shown in Figure 4B. The band gap of Pd-$Ga_2O_3$ was found to be 4.178 eV. According to recently published studies, β-$Ga_2O_3$ possesses the most stable crystal structure and a bandgap of around 4.8 eV (47). The previously reported band gap values of $Ga_2O_3$ nanowires using different catalysts such as Ni, Au, and Ag were 4.3, 4.7, and 4.4 eV, respectively (34,48,49). Compared to other catalysts described earlier, Pd doping with $Ga_2O_3$ NPs resulted in a greater decrease in band gap energy. The band gap of the $Ga_2O_3$ NPs was reduced by the addition of Pd.

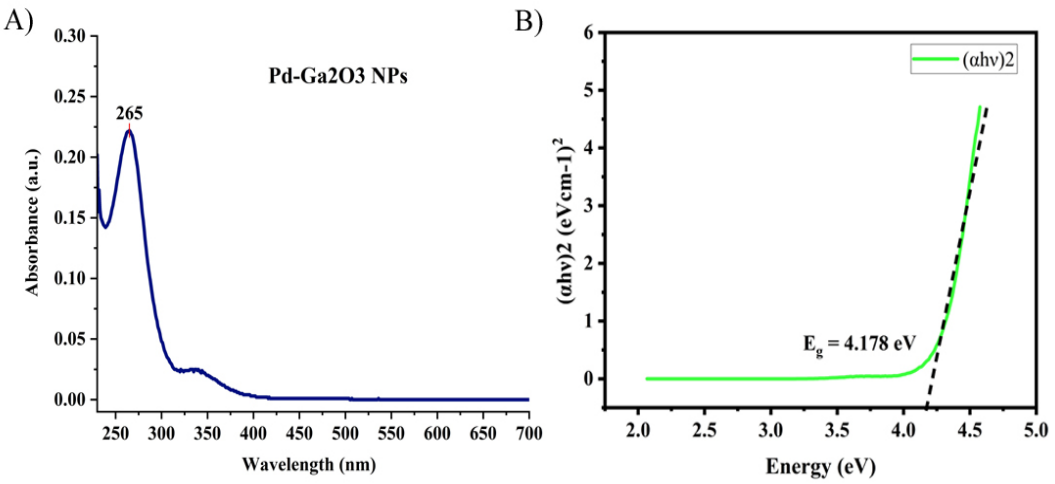


Figure 4: A) UV-Vis spectra of Pd-doped $Ga_2O_3$ NPs B) Band gap spectrum of Pd-$Ga_2O_3$- a plot of $(\alpha hv)^2$ against photon energy.

3.5 Pd-$Ga_2O_3$ inhibits the growth of microbes generated from medical waste

The photocatalytic activity of synthesised Pd-doped $Ga_2O_3$ NPs was evaluated against the microbiome generated from biomedical waste illustrated in Fig 5. The results indicated that Pd-$Ga_2O_3$ NPs completely prevented the growth of microorganisms. We employed the spread plate method, in which 1 ml of sample was initially diluted with 100 ml of distilled water and treated with Pd-$Ga_2O_3$ (5 mg/ml) for 2-3 hours, with untreated samples serving as a control. Both untreated and treated samples were serially diluted up to a $10^{-4}$ dilution and incubated for 24 hours. The results clearly revealed that microbe growth was observable in control plates (Fig. 5A-D), however Pd-$Ga_2O_3$ treatment entirely hindered microbe growth (Fig. 5E-H). The bar diagram (Fig. I) illustrates the quantitative number of colonies treated with Pd-Ga2O3 NPs as compared to the untreated control. As a result, the Pd-Ga2O3 NPs treatment is effective at reducing microbial growth in biomedical waste. As nano-photocatalysts are inexpensive, very stable, have a high photocatalytic activity, are safe for people, and many other advantages, They are widely used in the field of environmental and ecological safety for waste processing (1). Several methods have been employed to treat BMW, such as adsorption and ion exchange etc. However, the slow degrading efficacy, high cost, second contamination risk, and sophisticated technology of these approaches limit their use. Nano-photocatalysts are seen to be one of the most unique approaches for managing biomedical waste when it comes to energy consumption, ecological concerns, and environmental concerns, when compared to other approaches (50,51). Various photocatalysts, such as Metal oxides, including chromium, zinc, vanadium, cerium, and titanium oxides, are widely employed as photocatalysts due to their semiconducting characteristics. Metal oxide-based catalysts efficacy in photocatalytic oxidation is determined by criteria such as material crystallinity, phase, and size (52,53). Our findings are consistent with previous studies, which have demonstrated that Pd-$Ga_2O_3$ effectively inhibits the growth of various microorganisms, including bacteria and fungi. (54). This inhibitory impact is related to the gallium oxide ($Ga_2O_3$) component of Pd-$Ga_2O_3$, which has the potential to block iron. This disrupts the antioxidant system and inhibits microbial

growth and metabolism (42).

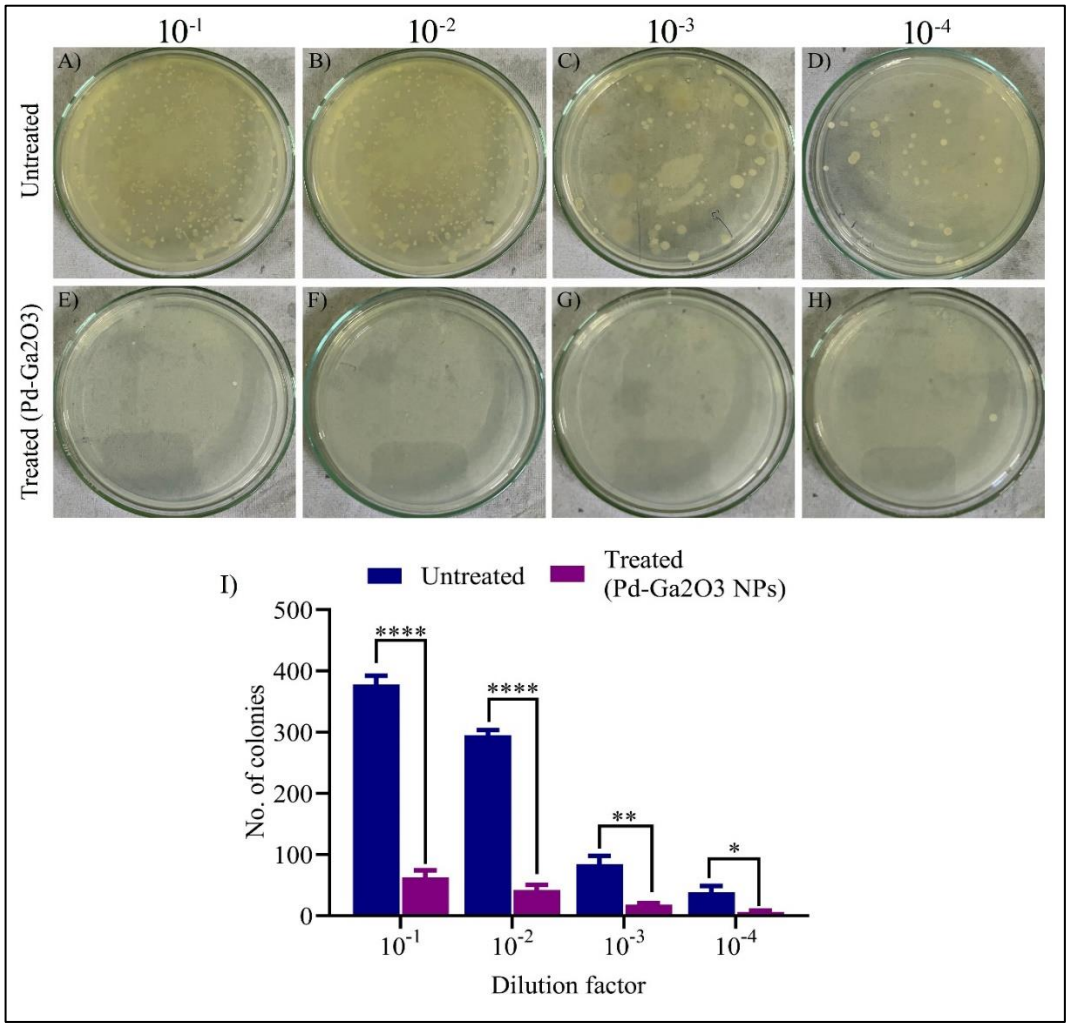


Figure 5: The effect of Pd-$Ga_2O_3$ on the growth of microbiota generated from biomedical waste: A)-D) Untreated samples were serially diluted (up to $10^{-4}$ dilutions) to clearly show the growth of microbial colonies. E)-H) The sample was treated for 2-3 hours with Pd-$Ga_2O_3$ (5 mg/ml). Following successive dilution (up to $10^{-4}$ dilutions) and incubation for 24 hours, the Pd-$Ga_2O_3$ treated sample showed clear inhibition of microbial growth. I) The bar graph shows quantitative the number of colonies treated with Pd-Ga2O3 NPs, relative to the untreated control. The statistical data is represented as Mean±SD. *P<0.05, **P<0.01, ****P<0.0001.

## 4. Conclusion

Pd-doped $Ga_2O_3$ NPs were effectively produced using the sol-gel method. The X-ray diffraction experiments reveal that Pd-doped $Ga_2O_3$ NPs form a single phase with a monoclinic

structure, with an average crystallite size of 15.11 nm. The SEM examination shows angular-shaped particles of Pd-$Ga_2O_3$ nanocomposite material with sizes ranging from 10-175 nm. Pd doping in $Ga_2O_3$ leads to a decrease in band gap, confirmed by UV-Visible spectroscopy. The photocatalytic activity of Pd-$Ga_2O_3$ was evaluated on microbiota produced from biomedical waste, and it clearly showed that the development of microorganisms derived from biomedical waste was significantly suppressed. The synthesized Pd-$Ga_2O_3$ NPs can prevent microbiological contamination at the small-scale level caused by BMW and so minimize contamination that affects the environment.

Acknowledgements:

The authors gratefully acknowledge financial support from the Science and Engineering

Research Board (SERB), Government of India, under Teacher Associateship for Research Excellence scheme; grant No: TAR/2022/000114 to DR D Suman. M. Vasundhara would like to acknowledge the support offered by Department of K&IM of Indian Institute of Chemical Technology (IICT/Pubs./2024/501).

Conflict of interest:

The authors declare that there is no conflict of interest regarding the publication of this

article.

**References**

1. Hooshmand S, Kargozar S, Ghorbani A, Darroudi M, Keshavarz M, Baino F, et al. Biomedical waste management by using nanophotocatalysts: The need for new options. Vol. 13, Materials. 2020.
2. Zhu L, Zhang Y, Yang Z, Li B, Feng T, Zou X, et al. Since January 2020 Elsevier has created a COVID-19 resource centre with free information in English and Mandarin on the novel coronavirus COVID- 19. The COVID-19 resource centre is hosted on Elsevier Connect, the company ' s public news and information. Intervirology. 2020;65(January):1–20.
3. WHO. Protecting Health Through Health Care Waste Management. 2016;4(4):379–88.
4. Central Pollution Control Board, Ministry of Forest Environment and Climate Change G of I. Annual Report on Biomedical Waste Management as per Biomedical Waste Management Rules, 2016 - For the year 2019. 2019;1–18. Available from: https://cpcb.nic.in/uploads/Projects/Bio-Medical-Waste/AR_BMWM_2019.pdf
5. Chand S, Shastry CS, Hiremath S, Joel JJ, Krishnabhat CH, Mateti UV. Updates on biomedical waste management during COVID-19: The Indian scenario. Clin Epidemiol Glob Heal [Internet]. 2021;11(February):100715. Available from: https://doi.org/10.1016/j.cegh.2021.100715
6. Capoor MR, Bhowmik KT. Current perspectives on biomedical waste management: Rules, conventions and treatment technologies. Indian J Med Microbiol. 2017;35(2):157–64.
7. Dermatas D, Mpouras T, Panagiotakis I. Application of Nanotechnology for waste management: Challenges and limitations. Waste Manag Res. 2018;36(3):197–9.
8. Joudeh N, Linke D. Nanoparticle classification, physicochemical properties, characterization, and applications: a comprehensive review for biologists. J Nanobiotechnology [Internet]. 2022;20(1):1–29. Available from: https://doi.org/10.1186/s12951-022-01477-8
9. Nascimento MA, Cruz JC, Rodrigues GD, de Oliveira AF, Lopes RP. Synthesis of polymetallic

NPs from spent lithium-ion batteries and application in the removal of reactive blue 4 dye. J Clean Prod. 2018;202:264–72.
10. Khan I, Saeed K, Khan I. NPs: Properties, applications and toxicities. Arab J Chem [Internet]. 2019;12(7):908–31. Available from: https://doi.org/10.1016/j.arabjc.2017.05.011
11. Stankic S, Suman S, Haque F, Vidic J. Pure and multi metal oxide NPs: Synthesis, antibacterial and cytotoxic properties. J Nanobiotechnology. 2016;14(1):1–20.
12. Rai M, Yadav A, Gade A. Silver nanoparticles as a new generation of antimicrobials. Biotechnol Adv [Internet]. 2009;27(1):76–83. Available from: http://dx.doi.org/10.1016/j.biotechadv.2008.09.002
13. Paszkiewicz M, Gołąbiewska A, Rajski Ł, Kowal E, Sajdak A, Zaleska-Medynska A. Synthesis and characterization of monometallic (Ag, Cu) and bimetallic Ag-Cu particles for antibacterial and antifungal applications. J Nanomater. 2016;2016.
14. Pasha A, Kumbhakar DV, Sana SS, Ravinder D. Role of Biosynthesized Ag-NPs Using Antimicrobial , Anti-Cancer and Anti-Angiogenic Activities. 2022;12(January):1–16.
15. Zare Y, Shabani I. Polymer/metal nanocomposites for biomedical applications. Mater Sci Eng C. 2016;60(28):195–203.
16. Basavegowda N, Baek KH. Multimetallic nanoparticles as alternative antimicrobial agents: Challenges and perspectives. Molecules. 2021;26(4).
17. Chiang JL, Yadlapalli BK, Chen MI, Wuu DS. A Review on Gallium Oxide Materials from Solution Processes. Nanomaterials. 2022;12(20).
18. Shi F, Qiao H. Preparations, properties and applications of gallium oxide nanomaterials – A review. Nano Sel. 2022;3(2):348–73.
19. Hasan MN, Lai J, Swinnich E, Zheng Y, Baboukani BS, Nalam PC, et al. Investigation of Nano-Gaps in Fractured β-$Ga_2O_3$ Nanomembranes Formed by Uniaxial Strain. Adv Electron Mater. 2021;7(2):1–9.
20. Pearton SJ, Yang J, Cary PH, Ren F, Kim J, Tadjer MJ, et al. A review of $Ga_2O_3$ materials, processing, and devices. Appl Phys Rev [Internet]. 2018;5(1). Available from: http://dx.doi.org/10.1063/1.5006941
21. Lu J, Xing J, Chen D, Xu H, Han X, Li D. Enhanced photocatalytic activity of β-$Ga_2O_3$ nanowires by Au nanoparticles decoration. J Mater Sci [Internet]. 2019;54(8):6530–41. Available from: https://doi.org/10.1007/s10853-019-03359-1
22. Reddy LS, Ko YH, Yu JS. Hydrothermal Synthesis and Photocatalytic Property of β-$Ga_2O_3$ Nanorods. Nanoscale Res Lett [Internet]. 2015;10(1). Available from: http://dx.doi.org/10.1186/s11671-015-1070-5
23. Arias A, Nedev N, Ghose S, Rojas-Ramirez JS, Mateos D, Alvarez MC, et al. Structural, optical, and electrical characterization of β-$Ga_2O_3$ thin films grown by plasma-assisted molecular beam epitaxy suitable for UV sensing. Adv Mater Sci Eng. 2018;2018.
24. Du F, Yang D, Sun Y, Jiao Y, Teng F, Fan H. Electrospun Zn-doped $Ga_2O_3$ nanofibers and their application in photodegrading rhodamine B dye. Ceram Int [Internet]. 2021;47(4):4963–71. Available from: https://doi.org/10.1016/j.ceramint.2020.10.072
25. Sudrajat H, Nguyen TK. Gallium oxide nanoparticles prepared through solid-state route for efficient photocatalytic overall water splitting. Optik (Stuttg) [Internet]. 2020;223(July):165370. Available from: https://doi.org/10.1016/j.ijleo.2020.165370
26. López I, Nogales E, Méndez B, Piqueras J, Peche A, Ramírez-Castellanos J, et al. Influence of sn and Cr doping on morphology and luminescence of thermally grown $Ga_2O_3$ nanowires. J Phys Chem C. 2013;117(6):3036–45.
27. Manandhar S, Battu AK, Orozco C, Ramana C V. Optical constants of titanium-doped gallium oxide thin films. Opt Mater (Amst) [Internet]. 2019;96(March):109223. Available from: https://doi.org/10.1016/j.optmat.2019.109223
28. Battu AK, Manandhar S, Shutthanandan V, Ramana C V. Controlled optical properties via

chemical composition tuning in molybdenum-incorporated B-$Ga_2O_3$ nanocrystalline films. Chem Phys Lett [Internet]. 2017;684:363–7. Available from: http://dx.doi.org/10.1016/j.cplett.2017.06.063

29. Venediktova OS, Bulavchenko OA, Afonasenko TN, Tsyrul'nikov PG, Vinokurov ZS, Chesalov YA, et al. Synthesis and characterization of mixed manganese-gallium oxides Mn3-xGaxO4 (x = 1–2) with the spinel structure. J Alloys Compd. 2017;725:496–503.
30. Zhang W, Naidu BS, Ou JZ, O'Mullane AP, Chrimes AF, Carey BJ, et al. Liquid metal/metal oxide frameworks with incorporated $Ga_2O_3$ for photocatalysis. ACS Appl Mater Interfaces. 2015;7(3):1943–8.
31. Wang X, Shen S, Jin S, Yang J, Li M, Wang X, et al. Effects of Zn2+ and Pb2+ dopants on the activity of $Ga_2O_3$-based photocatalysts for water splitting. Phys Chem Chem Phys. 2013;15(44):19380–6.
32. Sakata Y, Matsuda Y, Yanagida T, Hirata K, Imamura H, Teramura K. Effect of metal ion addition in a Ni supported $Ga_2O_3$ photocatalyst on the photocatalytic overall splitting of H2O. Catal Letters. 2008;125(1–2):22–6.
33. Hameed MM, Al-Samarai AME, Aadim KA. Synthesis and characterization of gallium oxide nanoparticles using pulsed laser deposition. Iraqi J Sci. 2020;61(10):2582–9.
34. Alhalaili B, Bunk RJ, Mao H, Cansizoglu H, Vidu R, Woodall J, et al. Gallium oxide nanowires for UV detection with enhanced growth and material properties. Sci Rep [Internet]. 2020;10(1):1–15. Available from: https://doi.org/10.1038/s41598-020-78326-x
35. Shaik EB, Kamal CS, Srinivasu K, Kumar BVN, Balla PK, Swamy RDK, et al. Optical insights of indium-doped β–$Ga_2O_3$ nanoparticles and its luminescence mechanism. J Mater Sci Mater Electron [Internet]. 2020;31(8):6185–91. Available from: https://doi.org/10.1007/s10854-020-03171-7
36. El-Fatah GA, Magar HS, Hassan RYA, Mahmoud R, Farghali AA, Hassouna MEM. A novel gallium oxide nanoparticles-based sensor for the simultaneous electrochemical detection of Pb2+, Cd2+ and Hg2+ ions in real water samples. Sci Rep [Internet]. 2022;12(1):1–14. Available from: https://doi.org/10.1038/s41598-022-24558-y
37. Vikal S, Gautam YK, Kumar A, Kumar A, Singh J, Pratap D, et al. Bioinspired palladium-doped manganese oxide nanocorns: a remarkable antimicrobial agent targeting phyto/animal pathogens. Sci Rep [Internet]. 2023;13(1):1–17. Available from: https://doi.org/10.1038/s41598-023-40822-1
38. Mallesham B, Roy S, Bose S, Nair AN, Sreenivasan S, Shutthanandan V, et al. Crystal Chemistry, Band-Gap Red Shift, and Electrocatalytic Activity of Iron-Doped Gallium Oxide Ceramics. ACS Omega. 2020;5(1):104–12.
39. Singh B, Arya S, Sharma A, Mahajan P, Gupta J, Singh A, et al. Effect of Pd concentration on the structural, morphological and photodiode properties of TiO2 nanoparticles. J Mater Sci Mater Electron [Internet]. 2020;31(1):65–74. Available from: http://dx.doi.org/10.1007/s10854-019-01095-5
40. Alhalaili B, Vidu R, Mao H, Islam MS. Comparative study of growth morphologies of $Ga_2O_3$ nanowires on different substrates. Nanomaterials. 2020;10(10):1–11.
41. Winkler N, Wibowo RA, Kautek W, Ligorio G, List-Kratochvil EJW, Dimopoulos T. Nanocrystalline $Ga_2O_3$ films deposited by spray pyrolysis from water-based solutions on glass and TCO substrates. J Mater Chem C. 2019;7(1):69–77.
42. Mohamed SH, El-Hagary M, Althoyaib S. Growth of β-Ga 2O 3 nanowires and their photocatalytic and optical properties using Pt as a catalyst. J Alloys Compd [Internet]. 2012;537:291–6. Available from: http://dx.doi.org/10.1016/j.jallcom.2012.05.048
43. Hassaan MA, El-Nemr MA, Elkatory MR, Ragab S, Niculescu VC, El Nemr A. Principles of Photocatalysts and Their Different Applications: A Review [Internet]. Vol. 381, Topics in Current Chemistry. Springer International Publishing; 2023. 1–54 p. Available from:

https://doi.org/10.1007/s41061-023-00444-7
44. Zuppella P, Pasqualotto E, Pasqualotto E, Zuccon S, Gerlin F, Corso AJ, et al. Palladium on plastic substrates for plasmonic devices. Sensors (Switzerland). 2015;15(1):1138–47.
45. Ghobadi N. Band gap determination using absorption spectrum fitting procedure. Int Nano Lett. 2013;3(1):2–5.
46. Makuła P, Pacia M, Macyk W. How To Correctly Determine the Band Gap Energy of Modified Semiconductor Photocatalysts Based on UV-Vis Spectra. J Phys Chem Lett. 2018;9(23):6814–7.
47. Ping LK, Berhanuddin DD, Mondal AK, Menon PS, Mohamed MA. Properties and perspectives of ultrawide bandgap $Ga_2O_3$ in optoelectronic applications. Chinese J Phys [Internet]. 2021;73(March):195–212. Available from: https://doi.org/10.1016/j.cjph.2021.06.015
48. Kumar M, Kumar V, Singh R. Diameter Tuning of β -$Ga_2O_3$ Nanowires Using Chemical Vapor Deposition Technique. Nanoscale Res Lett. 2017;12(1):1–10.
49. Kuo CL, Huang MH. The growth of ultralong and highly blue luminescent gallium oxide nanowires and nanobelts, and direct horizontal nanowire growth on substrates. Nanotechnology. 2008;19(15).
50. Al-Nuaim MA, Alwasiti AA, Shnain ZY. The photocatalytic process in the treatment of polluted water. Chem Pap [Internet]. 2023;77(2):677–701. Available from: https://doi.org/10.1007/s11696-022-02468-7
51. Jiang L, Wang Y, Feng C. Application of photocatalytic technology in environmental safety. Procedia Eng [Internet]. 2012;45:993–7. Available from: http://dx.doi.org/10.1016/j.proeng.2012.08.271
52. Tahir MB, Sohaib M, Sagir M, Rafique M. Role of Nanotechnology in Photocatalysis. Encycl Smart Mater. 2021;(January):578–89.
53. Tai XH, Lai CW, Juan JC, Lee KM. Nano-photocatalyst in photocatalytic oxidation processes [Internet]. Nanomaterials for Air Remediation. INC; 2020. 151–165 p. Available from: http://dx.doi.org/10.1016/B978-0-12-818821-7.00008-7
54. Shi F, Ma SS, Liu S, Xin R, Chen B, Ye W, et al. A novel antimicrobial strategy for bacterial infections: Gallium-based materials. Colloids Interface Sci Commun [Internet]. 2023;56(July):100735. Available from: https://doi.org/10.1016/j.colcom.2023.100735